doi:10.1038/nature13278

The poleward migration of the location of tropical cyclone maximum intensity

James P. Kossin[1], Kerry A. Emanuel[2] & Gabriel A. Vecchi[3]

Temporally inconsistent and potentially unreliable global historical data hinder the detection of trends in tropical cyclone activity[1–3]. This limits our confidence in evaluating proposed linkages between observed trends in tropical cyclones and in the environment[4,5]. Here we mitigate this difficulty by focusing on a metric that is comparatively insensitive to past data uncertainty, and identify a pronounced poleward migration in the average latitude at which tropical cyclones have achieved their lifetime-maximum intensity over the past 30 years. The poleward trends are evident in the global historical data in both the Northern and the Southern hemispheres, with rates of 53 and 62 kilometres per decade, respectively, and are statistically significant. When considered together, the trends in each hemisphere depict a global-average migration of tropical cyclone activity away from the tropics at a rate of about one degree of latitude per decade, which lies within the range of estimates of the observed expansion of the tropics over the same period[6]. The global migration remains evident and statistically significant under a formal data homogenization procedure[3], and is unlikely to be a data artefact. The migration away from the tropics is apparently linked to marked changes in the mean meridional structure of environmental vertical wind shear and potential intensity, and can plausibly be linked to tropical expansion, which is thought to have anthropogenic contributions[6].

Inconsistencies in the historical global 'best-track' data can introduce substantial uncertainty into global-mean measures of tropical cyclone activity. Since the introduction of geostationary weather satellites in the mid to late 1970s, measures of tropical cyclone frequency are generally considered to be accurate, and there is no observed trend in global frequency since that time[7,8]. Comparatively, measures of tropical cyclone intensity are considered to be highly uncertain in the global data[3,9]. Consequently, storm duration is also uncertain because identifying the moment when a cyclone forms (cyclogenesis) requires accuracy in intensity estimates, as the definition of cyclogenesis is entirely dependent on a nascent storm's intensity reaching a formally specified threshold. Similar uncertainty exists in identifying a cyclone's demise (cyclolysis). These uncertainties can project onto metrics such as power dissipation[10] and accumulated cyclone energy[11], which are amalgamations of frequency, duration and intensity.

But measurements of a storm's position taken around the time that it reaches its lifetime-maximum intensity (LMI) are much less uncertain. By this time in a storm's evolution, it is more likely to have been detected and to be under close observation. Measurements of storm position at the time of LMI are also less sensitive to inaccuracy in measurements of intensity, as well as to known interregional differences in wind-averaging techniques[9], because determining the absolute LMI is not critical—it is necessary only to know that the intensity has peaked. This also makes measurements of storm position at the time of LMI comparatively insensitive to temporal heterogeneity in the historical best-track intensity record[3]. It is this heterogeneity that has presented substantial challenges to trend detection in tropical cyclone metrics that require absolute measures of intensity[5].

Here we consider the 31-yr period 1982–2012. In this period, the global best-track data are considered most complete and at their highest quality in each basin[9], and storm position is well monitored globally by geostationary satellites. This period also encompasses a recent satellite-based global tropical cyclone intensity reanalysis[3], and is the interval over which the atmospheric reanalysis products[12–14] that provide information on the environmental changes that affect tropical cyclones are most reliable.

When the annual-mean latitude of LMI is calculated from the best-track data in the Northern and Southern hemispheres over this period (Fig. 1a, b, red lines), there are clear and statistically significant poleward trends in both hemispheres of 53 and 62 km per decade, respectively (Table 1). The positive contribution to these hemispheric trends from each ocean basin except that of the North Indian Ocean (Table 1 and Extended Data Fig. 1) suggests that the migration away from the tropics is a global phenomenon, although there are large regional differences in the trend amplitudes and their statistical power. These differences are probably due, in part, to regional differences in interannual to multidecadal variability[15]. The largest contribution to the Northern Hemisphere trend is from the western North Pacific Ocean, which is also the most active basin in terms of annual tropical cyclone frequency. By contrast, the North Indian Ocean has the lowest mean annual frequency, and the small equatorward trend there has a much lesser effect on the hemispheric trend. The North Atlantic Ocean and eastern North Pacific exhibit small poleward trends and also contribute little to the hemispheric trend. In the Southern Hemisphere, both the South Pacific and the South Indian Ocean regions contribute substantially to the poleward trend.

Within the period 1982–2009, the latitude of LMI can be reanalysed using a globally homogenized record of intensity (ADT-HURSAT[3]). When this is done, the annual-mean time series exhibit similar variability and trends (Fig. 1a, b, blue lines), although the ADT-HURSAT-based trend has a greater amplitude than the best-track-based trend in the Northern Hemisphere and a lesser amplitude than the best-track-based trend in the Southern Hemisphere (Table 1), where the trend is no longer significant with 95% confidence. However, when both hemispheres are considered together they depict a global migration away from the deep tropics, and the best-track and ADT-HURSAT data exhibit similar poleward trends of 115 and 118 km per decade, respectively (Table 1). In this global view, the trends in the best-track and ADT-HURSAT data are consistent and both are statistically significant.

As found with the best-track data, the ADT-HURSAT-based time series exhibit large differences in trend amplitudes and statistical power when separated by ocean basin (Table 1 and Extended Data Fig. 2). The western North Pacific is the largest contributor to the trend in the Northern Hemisphere, and the eastern North Pacific also contributes significantly, unlike the best-track data from that region. The equatorward trend in the North Indian Ocean best-track data is not found in the ADT-HURSAT data, which shows essentially no trend in that region (the lack of any poleward trend in the North Indian Ocean might be expected given the confines of the basin and the close proximity of land to the

[1]NOAA National Climatic Data Center, University of Wisconsin/CIMSS, 1225 West Dayton Street, Madison, Wisconsin 53706, USA. [2]Program in Atmospheres, Oceans, and Climate, Massachusetts Institute of Technology, Cambridge, Massachusetts 02139, USA. [3]NOAA Geophysical Fluid Dynamics Laboratory, Princeton, New Jersey 08540, USA.

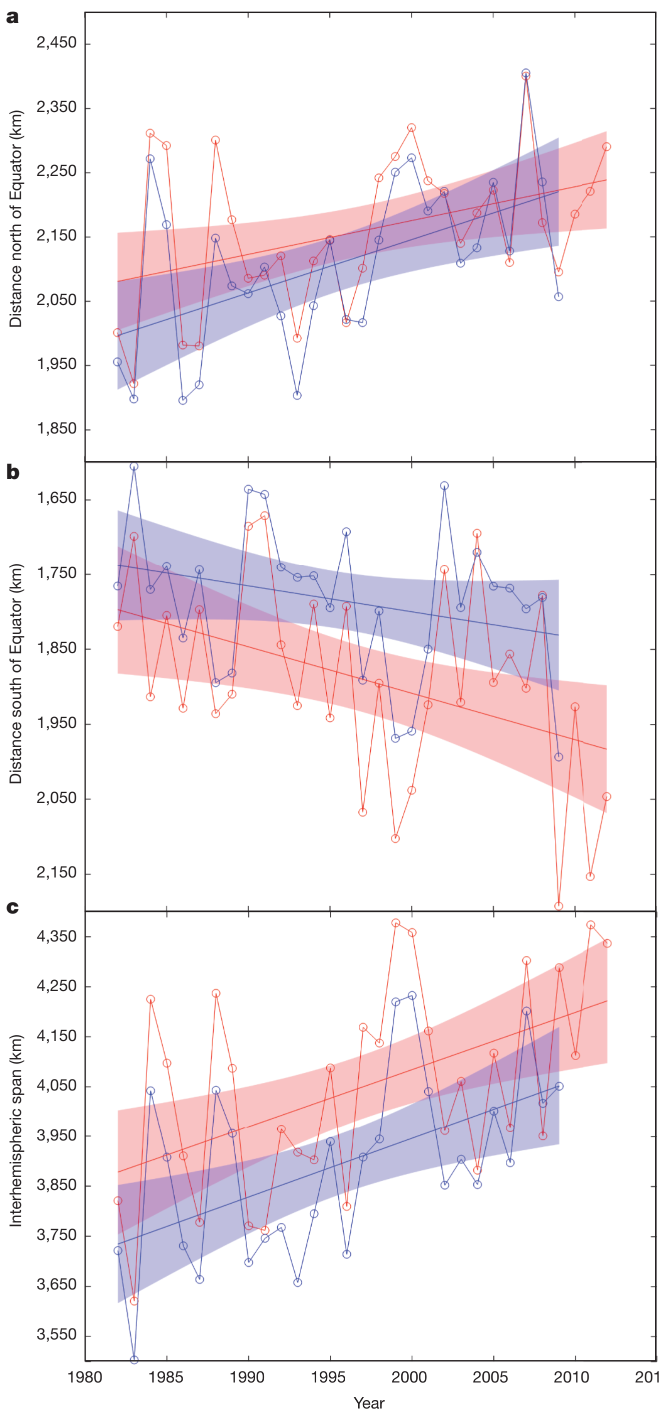

Figure 1 | Poleward migration of the latitude of LMI away from the tropics. **a**, **b**, Time series of annual-mean latitude of tropical cyclone LMI calculated from the best-track historical data (red) and the ADT-HURSAT reanalysis (blue) in the Northern (**a**) and Southern (**b**) hemispheres. **c**, The annual-mean difference between **a** and **b** shows the global migration of the latitude of LMI away from the tropics. Linear trend lines are shown with their 95% two-sided confidence intervals (shaded). Note that the *y* axis in **b** increases downwards.

north). In the North Atlantic, the best-track and ADT-HURSAT data sets both show essentially no trend. There are similar poleward trends in the best-track and ADT-HURSAT data from the South Pacific, but the ADT-HURSAT data in the South Indian Ocean exhibits a smaller, statistically insignificant trend.

Although regional differences are evident, the migration of the mean latitude of LMI away from the deep tropics is observed in both hemispheres, which indicates that this is a global phenomenon. The genesis and subsequent intensification period of tropical cyclones, which precedes LMI and controls when and where LMI occurs, is strongly modulated by the environment that the storms move through in this period. Known major factors controlling tropical cyclone evolution are the environmental vertical wind shear and the potential intensity[16–18]. Potential intensity describes the thermodynamically based maximum tropical cyclone intensity that the environment will support, all other factors being optimal. Vertical wind shear is one of the key factors that inhibit a storm from achieving this maximum. Greater shear and lesser potential intensity each inhibits genesis and intensification, and vice versa, and increased shear in the deep tropics, decreased shear at higher latitudes, or both, can thus be plausibly linked to a poleward migration of the latitude of LMI. Decreased potential intensity in the deep tropics, increased potential intensity at higher latitudes, or both, could be expected to result in a similar migration. Here we explore these environmental factors using three different atmospheric reanalysis products, NCEP/NCAR[12], ERA-Interim[13] and MERRA[14]. All three products exhibit broad regions of increased shear in the deep tropics and decreased shear in the subtropics (Fig. 2), which is consistent with the observed changes in the tropical cyclones. The changes in mean potential intensity are not as consistent among the different reanalysis products, particularly in the tropics, which is probably a result of spurious differences in upper tropospheric temperatures[19,20]. However, the meridional structure of potential intensity change is generally consistent in showing greater increases at higher latitudes, and the MERRA data, in particular, also show a broad reduction of potential intensity in the deep tropics.

The observed changes in shear and potential intensity provide evidence that the global migration of tropical cyclones away from the tropics is being modulated by systematic environmental changes. Shifts in tropical cyclone tracks in most regions have also been linked to phase changes in El Niño/Southern Oscillation[21–24] (ENSO), which can potentially contribute to the poleward trends in LMI identified here. To test this, we decrease the contribution of ENSO by regressing the LMI latitude time series onto an index of ENSO variability. When this is done (Fig. 3), the amplitude of the interhemispheric migration rates is found to decrease only slightly in both the best-track and the ADT-HURSAT data, and the statistical power of the trends in fact increases. This makes it unlikely that natural ENSO variability has a role in the observed multidecadal poleward migration of LMI, although it plays a substantial part in its interannual variability.

The potential for contributions from natural variability occurring on decadal or longer timescales still exists, but quantifying this is difficult using relatively short observation records. We propose that there is a linkage between the poleward migration of LMI and the observed expansion of the tropics. The rate of expansion since 1979 varies considerably among existing studies[6], but the rate of LMI migration identified here falls well within this range. This potential linkage between tropical cyclones and the expansion of the tropics further heightens interest in establishing the forcing mechanisms of the expansion, which are at present uncertain but are generally thought to have anthropogenic contributions[6]. The expansion of the tropics, as measured by the meridional

Table 1 | Linear trends, by region, of annual-mean latitude of LMI

	NHEM	SHEM	NATL	WPAC	EPAC	NIO	SIO	SPAC	Global
Best track	+53 ± 43	+62 ± 48	+7 ± 98	+37 ± 55	+10 ± 32	−25 ± 78	+67 ± 55	+51 ± 68	+115 ± 70
ADT-HURSAT	+83 ± 50	+35 ± 44	−12 ± 126	+105 ± 71	+34 ± 30	+10 ± 106	+30 ± 52	+54 ± 79	+118 ± 70

Trends are deduced from the best-track and ADT-HURSAT data sets. The slope (kilometres per decade) and the 95% two-sided confidence bounds are shown. Positive slopes represent poleward migration. NHEM, Northern Hemisphere; SHEM, Southern Hemisphere; NATL, North Atlantic; WPAC, western Pacific; EPAC, eastern Pacific; NIO, North Indian Ocean; SIO, South Indian Ocean; SPAC, South Pacific.

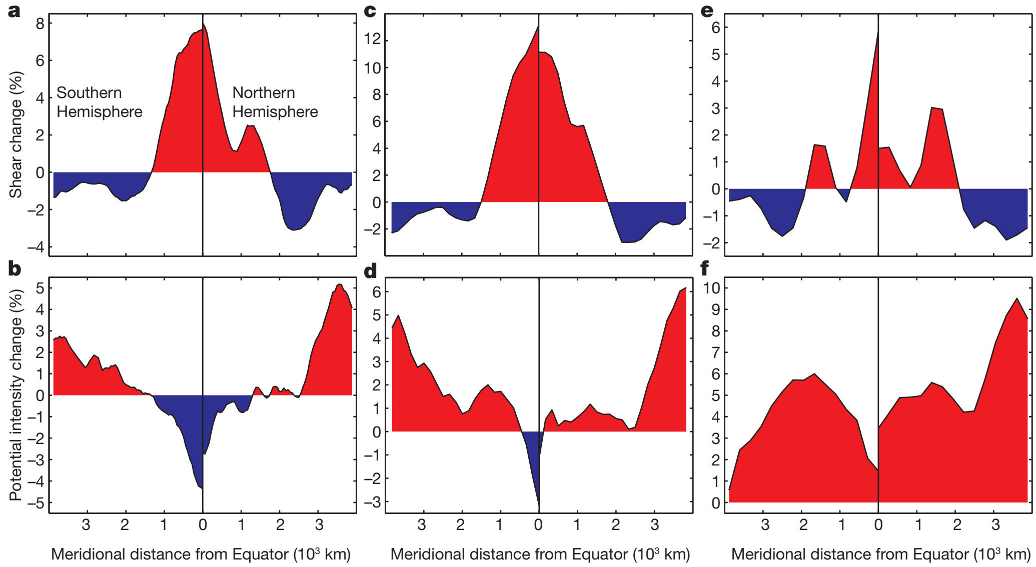

Figure 2 | Observed changes in the mean environment where tropical cyclones form and track. Percentage changes from 1980–1994 to 1995–2010 in mean vertical wind shear (**a**, **c**, **e**) and potential intensity (**b**, **d**, **f**). Annual means are taken over the peak tropical cyclone seasons in each hemisphere (August–October in the north and January–March in the south) from three different reanalysis products: MERRA (**a**, **b**), ERA-Interim (**c**, **d**) and NCEP/NCAR (**e**, **f**).

extent of the tropical Hadley circulation, exhibits a step change in the late 1990s[6]. Formal change-point analysis applied to the global time series of LMI latitude reveals a significant change point in 1996, providing further support for a linkage between the two independently observed phenomena.

Observed changes in vertical wind shear and potential intensity over the past 30 yr seem to have resulted in a poleward shift, in both hemispheres, of the regions most favourable for tropical cyclone development (Fig. 2), and an associated migration of tropical cyclone activity away from the tropics (Fig. 1). If these environmental changes continue, a concomitant continued poleward migration of the latitude where tropical cyclones achieve their LMI would have potentially profound consequences for life and property. Any related changes in positions where storms make landfall will have obvious effects on coastal residents and infrastructure. Increasing hazard exposure and mortality risk from tropical cyclones[25] may be compounded in coastal cities outside the tropics, while being offset at lower latitudes. Tropical cyclones also have an important role in maintaining regional water resources[26,27], and a poleward migration of storm tracks could threaten potable water supplies in some regions while increasing flooding events in others. Given these motivating factors, further study of the poleward migration of tropical cyclone LMI identified here, and its potential link to the observed expansion of the tropics, is warranted.

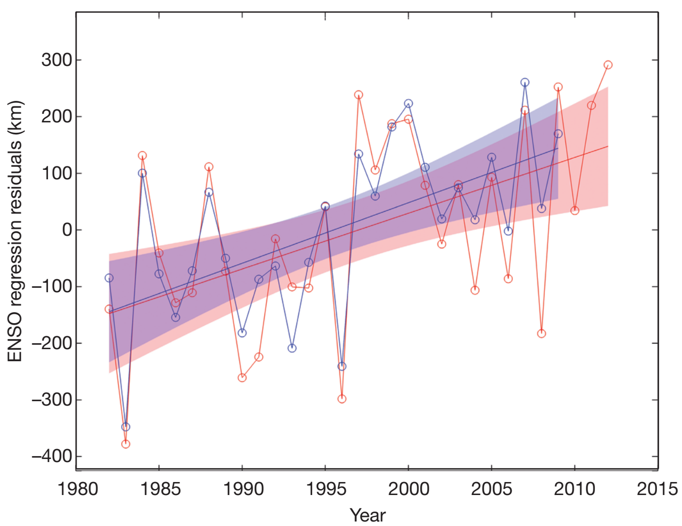

Figure 3 | Global trends of the latitude of LMI with ENSO variability reduced. Time series of the latitude of LMI calculated from the best-track historical data (red; trend, 99 ± 59 km per decade) and the ADT-HURSAT reanalysis (blue; trend, 107 ± 53 km per decade) with ENSO variability reduced. The values are calculated from residuals of the regression of LMI latitude onto an index of ENSO variability. Shading represents the 95% two-sided confidence interval of the trend.

METHODS SUMMARY

Best-track data were taken from the International Best Track Archive for Climate Stewardship (IBTrACS) v03r05 (ref. 28). Following ref. 3, when a storm has overlapping data from multiple sources, we used the source with the greatest reported LMI. The homogenized intensity data were taken from the Advanced Dvorak Technique Hurricane Satellite (ADT-HURSAT) data set[3]. Vertical wind shear and potential intensity were calculated over water in the region spanning latitudes 35° S to 35° N. In the Southern Hemisphere, the longitude was confined to 30°–240° E, which excludes the region where storms are not observed to form or track. The wind shear is estimated as the magnitude of the vector difference of the respective horizontal wind velocities at the 250- and 850-hPa pressure levels. Potential intensity was calculated following ref. 29. ENSO variability was decreased in the LMI latitude time series by regressing the series from the two hemispheres onto the Niño-3.4 index[30] averaged over the most active periods of tropical cyclone activity (August–October in the north and January–March in the south), and analysing the residuals. None of the time series studied in this paper exhibited autocorrelation after detrending, as determined with the Durbin–Watson test statistic, and no corrections were necessary when calculating the confidence intervals.

Online Content Any additional Methods, Extended Data display items and Source Data are available in the online version of the paper; references unique to these sections appear only in the online paper.

Received 21 October 2013; accepted 21 March 2014.

1. Landsea, C. W., Vecchi, G. A., Bengtsson, L. & Knutson, T. R. Impact of duration thresholds on Atlantic tropical cyclone counts. *J. Clim.* **23,** 2508–2519 (2010).
2. Vecchi, G. A. & Knutson, T. R. Estimating annual numbers of Atlantic hurricanes missing from the HURDAT database (1878–1965) using ship track density. *J. Clim.* **24,** 1736–1746 (2011).
3. Kossin, J. P., Olander, T. L. & Knapp, K. R. Trend analysis with a new global record of tropical cyclone intensity. *J. Clim.* **26,** 9960–9976 (2013).
4. Knutson, T. R. *et al.* Tropical cyclones and climate change. *Nature Geosci.* **3,** 157–163 (2010).

5. Seneviratne, S. I. *et al.* in *Managing the Risks of Extreme Events and Disasters to Advance Climate Change Adaptation* (eds Field, C. B. *et al.*) 109–230 (Cambridge Univ. Press, 2012).
6. Lucas, C., Timbal, B. & Nguyen, H. The expanding tropics: a critical assessment of the observational and modeling studies. *WIREs. Clim. Change* **5,** 89–112 (2014).
7. Frank, W. M., &. Young, G. S. The interannual variability of tropical cyclones. *Mon. Weath. Rev.* **135,** 3587–3598 (2007).
8. Holland, G. & Bruyere, C. L. Recent intense hurricane response to global climate change. *Clim. Dyn.* **42,** 617–627 (2013).
9. Knapp, K. R. & Kruk, M. C. Quantifying interagency differences in tropical cyclone best track wind speed estimates. *Mon. Weath. Rev.* **138,** 1459–1473 (2010).
10. Emanuel, K. A. Increasing destructiveness of tropical cyclones over the past 30 years. *Nature* **436,** 686–688 (2005).
11. Bell, G. D. *et al.* Climate assessment for 1999. *Bull. Am. Meteorol. Soc.* **81,** s1–s50 (2000).
12. Kalnay, E. *et al.* The NCEP/NCAR 40-year reanalysis project. *Bull. Am. Meteorol. Soc.* **77,** 437–471 (1996).
13. Dee, D. P. *et al.* The ERA-Interim reanalysis: configuration and performance of the data assimilation system. *Q. J. R. Meteorol. Soc.* **137,** 553–597 (2011).
14. Rienecker, M. *et al.* MERRA: NASA's Modern-Era Retrospective Analysis for Research and Applications. *J. Clim.* **24,** 3624–3648 (2011).
15. Bindoff, N. L. *et al.* in *Climate Change 2013: The Physical Science Basis* (eds Stocker, T. F. *et al.*) 867–952 (Cambridge Univ. Press, 2013).
16. Knaff, J. A., Seseske, S. A., DeMaria, M. & Demuth, J. L. On the influences of vertical wind shear on symmetric tropical cyclone structure derived from AMSU. *Mon. Weath. Rev.* **132,** 2503–2510 (2004).
17. Zhang, F. & Tao, D. Effects of vertical wind shear on the predictability of tropical cyclones. *J. Atmos. Sci.* **70,** 975–983 (2013).
18. Emanuel, K. A. Thermodynamic control of hurricane intensity. *Nature* **401,** 665–669 (1999).
19. Vecchi, G. A., Fueglistaler, S., Held, I. M., Knutson, T. R. & Zhao, M. Impacts of atmospheric temperature trends on tropical cyclone activity. *J. Clim.* **26,** 3877–3891 (2013).
20. Emanuel, K., Solomon, S., Folini, D., Davis, S. & Cagnazzo, C. Influence of tropical tropopause layer cooling on Atlantic hurricane activity. *J. Clim.* **26,** 2288–2301 (2013).
21. Camargo, S. J., Robertson, A. W. & Gaffney, S. J. Smyth, P. & Ghil, M. Cluster analysis of typhoon tracks. Part II: large-scale circulation and ENSO. *J. Clim.* **20,** 3654–3676 (2007).
22. Camargo, S. J., Robertson, A. W., Barnston, A. G. & Ghil, M. Clustering of eastern North Pacific tropical cyclone tracks: ENSO and MJO effects. *Geochem. Geophys. Geosyst.* **9,** Q06V05 (2008).
23. Kossin, J. P., Camargo, S. J. & Sitkowski, M. Climate modulation of North Atlantic hurricane tracks. *J. Clim.* **23,** 3057–3076 (2010).
24. Ramsay, H. A., Camargo, S. J. & Kim, D. Cluster analysis of tropical cyclone tracks in the Southern Hemisphere. *Clim. Dyn.* **39,** 897–917 (2012).
25. Peduzzi, P. *et al.* Tropical cyclones: global trends in human exposure, vulnerability and risk. *Nature Clim. Change* **2,** 289–294 (2012).
26. Jiang, H. & Zipser, E. Contribution of tropical cyclones to the global precipitation from eight seasons of TRMM data: regional, seasonal, and interannual variations. *J. Clim.* **23,** 1526–1543 (2010).
27. Lam, H., Kok, M. H. & Shum, K. K. Y. Benefits from typhoons – the Hong Kong perspective. *Weather* **67,** 16–21 (2012).
28. Knapp, K. P., Kruk, M. C., Levinson, D. H., Diamond, H. J. & Neumann, C. J. The International Best Track Archive for Climate Stewardship (IBTrACS): unifying tropical cyclone data. *Bull. Am. Meteorol. Soc.* **91,** 363–376 (2010).
29. Bister, M. & Emanuel, K. A. Dissipative heating and hurricane intensity. *Meteorol. Atmos. Phys.* **65,** 233–240 (1998).
30. Barnston, A. G., Chelliah, M. & Goldenberg, S. B. Documentation of a highly ENSO-related SST region in the equatorial Pacific. *Atmosphere–Ocean* **35,** 367–383 (1997).

Author Contributions J.P.K. had the idea for, and designed, the study, and performed the analyses with input from K.A.E. and G.A.V. J.P.K., K.A.E. and G.A.V. provided data and participated in interpretation of the results and the writing of the manuscript.

Author Information Reprints and permissions information is available at www.nature.com/reprints. The authors declare no competing financial interests. Readers are welcome to comment on the online version of the paper. Correspondence and requests for materials should be addressed to J.P.K. (james.kossin@noaa.gov).

METHODS

Best-track data were taken from the International Best Track Archive for Climate Stewardship (IBTrACS) v03r05 (ref. 28) and are available at http://www.ncdc.noaa.gov/ibtracs/. Following ref. 3, when a storm has overlapping data from multiple sources, we used the source with the greatest reported LMI. In storms that achieve their LMI more than once, the latitude of LMI is taken at the first occurrence. The homogenized intensity data were taken from the Advanced Dvorak Technique Hurricane Satellite (ADT-HURSAT) data set[3]. The data reflect the additional homogenization procedure addressing the discontinuity in satellite coverage that occurred in 1997. The global distribution of the ADT-HURSAT LMI is known to be spuriously leptokurtic[3], which is the likely cause of the consistent equatorward bias in the mean latitude of LMI when compared to the best-track data, but there is no expectation that this bias has any time dependence and it is not expected to affect the trends.

ENSO variability was removed from the LMI latitude time series by regressing the individual series from the Northern and Southern hemispheres onto the Niño-3.4 index[30] averaged over the most active periods of tropical cyclone activity (August–October in the north and January–March in the south), and analysing the residuals. The index is available at http://www.cpc.ncep.noaa.gov/data/indices/.

None of the time series explored in this paper exhibits autocorrelation after detrending, as determined with the Durbin–Watson test statistic, and no corrections were necessary when calculating the confidence intervals. In addition to linear trend analysis, the time series were explored for change points with models based on batch detection using both the Student t and Mann–Whitney statistics to test for significance at 95% confidence or greater using the 'cpm' package[31] in the software environment R.

The global trends in the annual mean latitude of LMI are a result of both intrabasin and interbasin changes. The climatological mean latitude of LMI varies by basin (see, for example, Extended Data Fig. 1) such that, in addition to meridional shifts within each basin, changes in the relative annual frequency of storms from each basin can also contribute to the global trends in the latitude of LMI. To quantify this contribution, the LMI latitude of every storm was normalized by the respective basin-mean LMI latitude, and the analysis of Fig. 1c was repeated. When this was performed, the trend in the best-track data decreased from 115 ± 70 to 78 ± 66 km per decade and the trend in the ADT-HURSAT data decreased from 118 ± 70 to 92 ± 65 km per decade. Thus, both factors contribute, but the intrabasin poleward migration of LMI dominates the trends.

Monthly-mean vertical wind shear and potential intensity were calculated over water in the region spanning latitudes 35° S–35° N. In the Southern Hemisphere, the longitude was confined to 30°–240° E, which excludes the region where storms are not observed to form or track. Vertical wind shear was calculated as[32]

$$\text{shear} = \left\{ (\bar{u}_{250} - \bar{u}_{850})^2 + (\bar{v}_{250} - \bar{v}_{850})^2 + \overline{u'^2_{250}} + \overline{v'^2_{250}} + \overline{u'^2_{850}} + \overline{v'^2_{850}} - 2\left(\overline{u'_{250}u'_{850}} + \overline{v'_{250}v'_{850}}\right) \right\}^{1/2}$$

where u_{250}, u_{850}, v_{250} and v_{850} are the zonal (u) and meridional (v) winds at the 250- and 850-hPa pressure levels; u'_{250}, u'_{850}, v'_{250} and v'_{850} are departures of the corresponding daily means from their monthly means; and overbars represent monthly-mean quantities. Potential intensity was calculated following ref. 29. In the Northern Hemisphere the shear and potential intensity were averaged over August–October, and in the Southern Hemisphere they were averaged over January–March.

31. Ross, G. J. cpm: sequential parametric and nonparametric change detection. R package version 1.1. http://CRAN.R-project.org/package=cpm (2013).
32. Emanuel, K. Tropical cyclone activity downscaled from NOAA-CIRES reanalysis, 1908–1958. *J. Adv. Model. Earth Syst.* **2,** 1 (2010).

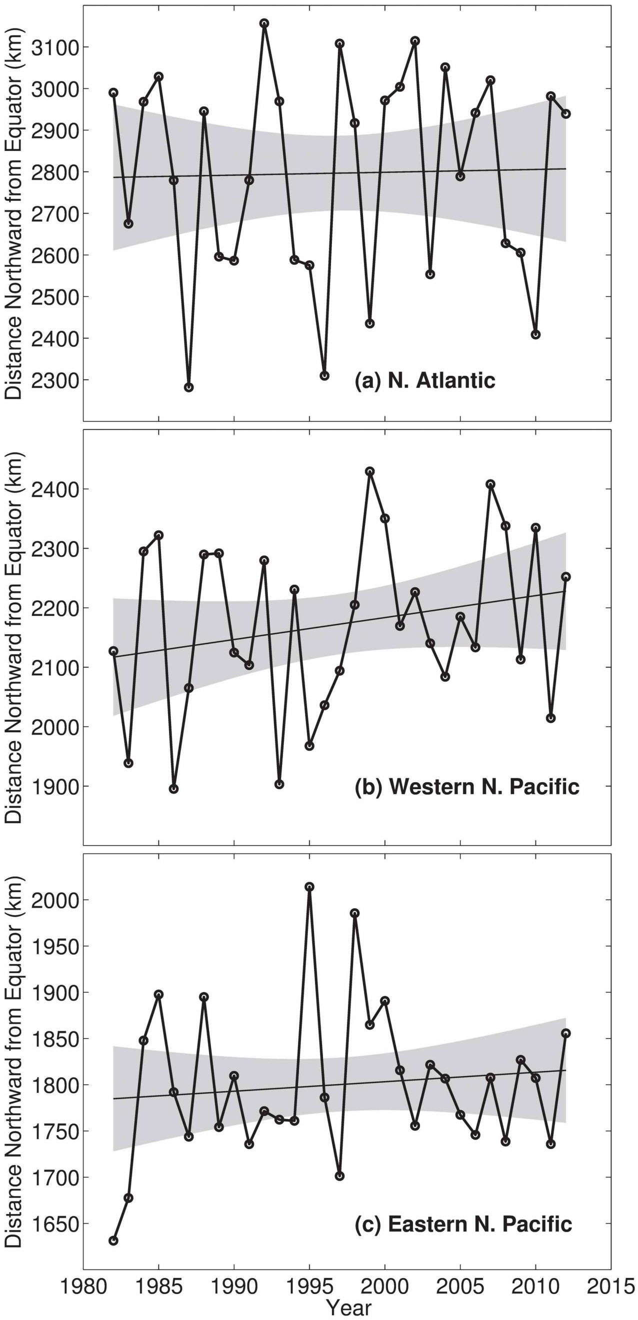

Extended Data Figure 1 | Time series of annual-mean latitude of LMI calculated from the best-track historical data from each ocean basin. The basins are those in the North Atlantic (**a**), the western North Pacific (**b**), the eastern North Pacific (**c**), the Northern Indian Ocean (**d**), the Southern Indian Ocean (**e**) and the South Pacific (**f**). Linear trend lines are shown with their 95% two-sided confidence intervals (shaded). Note that the *y* axes in **e** and **f** increase downwards.

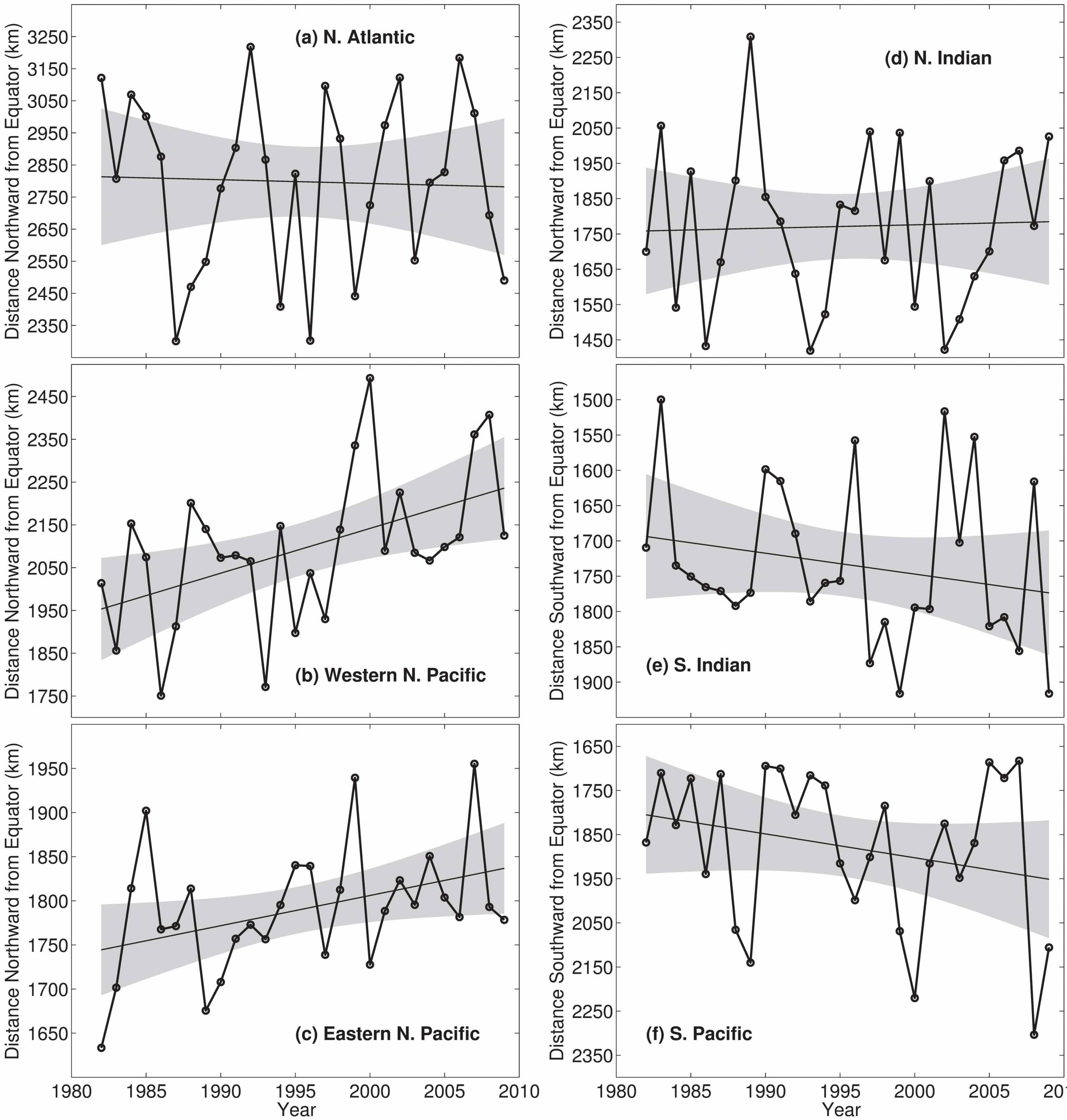

Extended Data Figure 2 | Time series of annual-mean latitude of LMI calculated from the ADT-HURSAT data from each ocean basin. The basins are those in the North Atlantic (**a**), the western North Pacific (**b**), the eastern North Pacific (**c**), the Northern Indian Ocean (**d**), the Southern Indian Ocean (**e**) and the South Pacific (**f**). Linear trend lines are shown with their 95% two-sided confidence intervals (shaded). Note that the *y* axes in **e** and **f** increase downwards.